Journal of Non-Crystalline Solids 401 (2014) 73–77

Contents lists available at ScienceDirect

Journal of Non-Crystalline Solids

journal homepage: www.elsevier.com/ locate/ jnoncrysol

# Glass-like dynamics of new cross-linked polymeric systems: Behavior of the Boson peak

B. Rossi [a,*], A. Fontana [a], M. Giarola [b], G. Mariotto [b], A. Mele [c], C. Punta [c], L. Melone [c], F. Toraldo [c], F. Trotta [d]

[a] Department of Physics, University of Trento, via Sommarive 14, 38123 Povo (Trento), Italy
[b] Department of Computer Science, University of Verona, Strada le Grazie 15, 37134 Verona, Italy
[c] Department of Chemistry, Materials and Chemical Engineering "G. Natta", Politecnico di Milano, Via Mancinelli 7, 20131 Milano, Italy
[d] Department of Chemistry, University of Torino, Via Pietro Giuria 7, 10125 Torino, Italy

ARTICLE INFO

*Article history:*
Received 12 July 2013
Received in revised form 23 December 2013
Available online 21 January 2014

*Keywords:*
Cross-linked polymers;
Cyclodextrin;
Boson peak;
Raman scattering;
Nanostructured materials

ABSTRACT

Cyclodextrin nanosponges (CDNS) provide a very promising class of cross-linked polymers consisting of cyclodextrins as building blocks and showing a characteristic nanoporous structure capable of effectively encapsulating and carrying a variety of both lipophilic and hydrophilic compounds. Hereafter, we investigate the vibrational dynamics of CDNS in the low-wave number region, with the aim to provide physical descriptors correlated to the elastic properties of this innovative glass-forming material. By means of Raman scattering measurements, we explore the modifications occurring to the boson peak (BP) as a function of the cavity size of the cyclodextrin and the relative amount of the cross-linking agent with respect to the monomer cyclodextrin, which can be varied during the synthesis of the polymer. The shift and intensity variations of the BP are discussed in terms of the modification of the elastic properties of CDNS, and a master curve for the boson peak can therefore be obtained. The experimental approach adopted here is a useful tool for investigating the structural and physico-chemical properties of novel nanoporous soft materials of interest for biolife applications.



## 1. Introduction

Cyclodextrin nanosponges (CDNS) represent a very promising class of cross-linked polymers showing a unique three-dimensional architecture that consists of both hydrophilic and hydrophobic nanosized pores, where a large variety of guest compounds can be effectively encapsulated [1–3]. The monomeric units of CDNS are constituted by cyclodextrins (CD), natural cyclic oligosaccharides formed by 6–8 glucose units linked by 1,4-α-glycosidic bonds leading to form α-, β-, and γ-CD, respectively. CD show a characteristic structure of a truncated cone, with an internal hydrophobic cavity and an outer hydrophilic surface [4–6], and they are well known for their capability of including a large variety of organic compounds via non-covalent interactions. The reaction of polymerization of CD with suitable polyfunctional agents leads to highly cross-linked amorphous structures, referred to as cyclodextrin nanosponges, characterized by unique molecular encapsulation properties. These polymeric networks play a key role in the rational design of new soft materials for application as carrier systems in many different technological fields, including agriculture [7], environmental control [8] cosmetic and pharmaceutical domain [9–14].

In this scenario, the deep knowledge of the architecture of the network connectivity or an estimation of the cross-linking density of CDNS is a crucial step to understand how the molecular structure can affect the functional properties of these polymers. This is an important challenge in view of the possibility to control and tune the molecular encapsulation ability inside the matrix of these very promising amorphous systems. On the other hand, despite the easy synthesis and the versatility of CDNS, carrying out a systematic structural and dynamic characterization of cross-linked polymeric networks suffers from many intrinsic difficulties, mainly due to the random nature of the growing process which leads to the formation of the polymer.

Recent experimental-numerical works [15–20] showed how the study of the vibrational dynamics of CDNS is a powerful tool to characterize amorphous polymeric networks, from a structural point of view, too. The detailed analysis of the high-frequency vibrational dynamics of nanosponges revealed a clear dependence of the hydrogen-bonded network involving the OH groups of the polymers on the temperature and on the cross-linking degree of CDNS [20]. Moreover, the inspection of the vibrational spectra of the polymers over a broad spectral range [15–19] allowed us to demonstrate that the cross-linking density of the polymeric network and the stiffness (i.e., rigidity) of the whole material can be effectively tuned by varying the chemical structure of cross-linking agent and the reaction conditions. In particular, the relative amount of crosslinking agent with respect to the monomer CD (i.e., $n$ = crosslinking agent/CD molar ratio) was observed to be the parameter which mainly can affect the covalent connectivity [17–19] and the elastic properties of the polymeric matrix [15–17].

In this paper, the low-energy vibrational excitations of cyclodextrin nanosponges, obtained by polymerization of α- and γ-CD with the

* Corresponding author.
*E-mail address:* rossi@science.unitn.it (B. Rossi).

0022-3093/$ – see front matter © 2014 Elsevier B.V. All rights reserved.
http://dx.doi.org/10.1016/j.jnoncrysol.2014.01.016

cross-linking agent ethylenediaminetetraacetic acid (EDTA), are investigated by means of Raman scattering experiments. The structure of α- and γ-CD differs by the number of glucose units, composed of macrocycle (6 and 8, respectively), and this is reflected in a different size of the cavity diameter of the CD (≈4.7 and 7.5 Å for α- and γ-CD, respectively). The aim of this work is exploring as how the steric hindrance and the number of reactive sites on each CD unit (which varies from 12 secondary and 6 primary OH groups to 16 secondary and 8 primary groups per CD residue passing from α-CD to γ-CD) can affect the stiffness properties of the polymer network over a mesoscopic length scale. For this purpose, the spectral evolution of the so-called Boson peak (BP), a vibrational feature usually observed in the low-energy vibrational spectra of a wide range of different amorphous materials [21–24], will be analyzed and discussed in terms of a physical descriptor correlated to the elasticity properties of these amorphous polymeric networks [16,17].

## 2. Experimental methods

### 2.1. Synthesis and purification of nanosponges

The nanosponges were obtained following a synthetic procedure previously reported [1,2,25]. In order to obtain α-CDEDTA1*n* and γ-CDEDTA1*n* nanosponges, anhydrous α-CD (γ-CD) was dissolved at room temperature in anhydrous DMSO containing 1 mL of anhydrous $Et_3N$. Then the cross-linking agent ethylenediaminetetraacetic acid dianhydride (EDTAn) was added at molecular ratios of 1:*n* (with $n = 2, 6, 10$) under intense stirring. The polymerization was complete in few minutes obtaining a solid that was broken up with a spatula and washed with acetone in a Soxhlet apparatus for 24 h. The pale yellow solid was finally dried under vacuum obtaining finally an apparently homogeneous powder.

### 2.2. Raman scattering measurements

All the Raman measurements were carried out at room temperature from dried specimens of nanosponges placed on a glass slide exposed to air. Cross-polarized (HV) anti-Stokes and Stokes Raman spectra were recorded over the wave number range between about $-400$ cm$^{-1}$ and $+370$ cm$^{-1}$ in backscattering geometry, by means of a triple-monochromator spectrometer (Horiba-Jobin Yvon, model T64000) set in double-subtractive/single configuration and mounting three holographic gratings with 1800 grooves/mm. Micro-Raman spectra were excited by the 632.8-nm wavelength of a helium/neon or by the 647.1-nm wavelength of an argon/krypton ion laser and detected by a multichannel detector (CCD with 1024 × 256 pixels) cryogenically cooled by liquid nitrogen. The laser beam was focused onto the sample surface with a spot size of about 1 μm$^2$ through an 80× objective of the microscope with NA = 0.75. The resolution was better than 0.4 cm$^{-1}$/pixel.

No appreciable damage due to possible heating of the sample was observed by means of an accurate inspection of the irradiated sample surface throughout the camera coupled to the microscope objective and carried out after each measurement. Moreover, four Raman spectra were recorded from different regions of each examined sample in order to verify their reproducibility.

## 3. Results

Cross-polarized Raman intensity $I_{Raman}(\omega,T)$ of α-CDEDTA110 nanosponge is shown in the wave number region between $+200$ cm$^{-1}$ and $-200$ cm$^{-1}$ (Fig. 1). The experimental profile shows two different contributions, which appear evident in both the anti-Stokes and Stokes components of the spectrum: a quasi-elastic (QE) signal, related to diffusive and relaxational dynamics of the system, which appears as a broadening of the elastic peak, and the broad bump, characteristic of disordered systems, usually referred as the boson peak (BP).

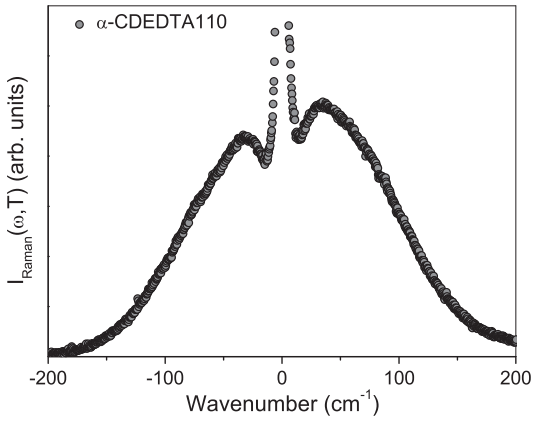


**Fig. 1.** Cross-polarized (HV) Raman intensity $I^{HV}_{Raman}$ of α-CDEDTA110 nanosponge in the wave number region between $+200$ cm$^{-1}$ and $-200$ cm$^{-1}$.

According to Shuker and Gammon model [26], the experimental intensity $I_{Raman}(\omega,T)$ of Raman scattering Stokes processes turns out to be proportional to the density of states $g(\omega)$ through the following relation:

$$I_{Raman}(\omega,T) = C(\omega)g(\omega)\frac{[n(\omega,T)+1]}{\omega} \quad (1)$$

where $n(\omega,T) = [\exp(\hbar\omega/kT) - 1]^{-1}$ is the temperature Bose factor and $C(\omega)$ is the coupling function between light and vibrational mode of frequency $\omega$ of the system.

In order to rule out the temperature dependence of the Raman spectra, the measured intensity can be converted into the reduced Raman intensity, defined as

$$I^{Red}(\omega) = \frac{I_{Raman}(\omega,T)}{[n(\omega,T)+1]\omega} = C(\omega)\frac{g(\omega)}{\omega^2} \quad (2)$$

The reduced Raman intensity $I^{Red}(\omega)$ derived from the Stokes component of the cross-polarized spectrum of three different α-CDEDTA1*n* nanosponges in the low-energy region (0–200 cm$^{-1}$) is shown in Fig. 2, as an example.

In order to compare Raman spectra acquired on different samples of EDTA nanosponges, the experimental data were preliminary normalized to the total measured area.

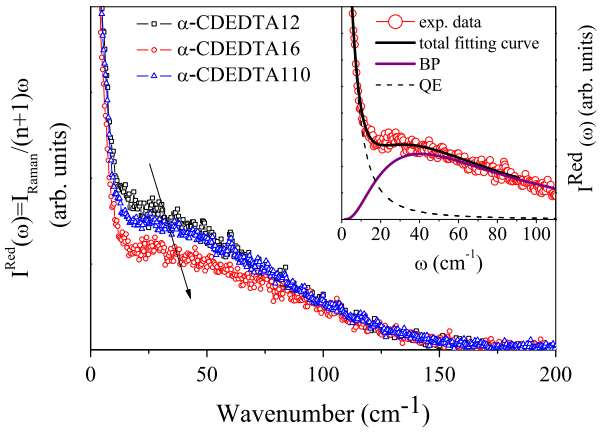


**Fig. 2.** Reduced Raman spectra of α-CDEDTA1*n* nanosponges ($n = 2, 6, 10$) in the energy range 0–200 cm$^{-1}$; the arrow indicates the evolution of the BP peak frequency. (Inset) Typical example of the best fitting results for α-CDEDTA16: the experimental data (red circles) are shown together with the total fitting curve and the different components (QE, quasi-elastic; BP, boson peak).

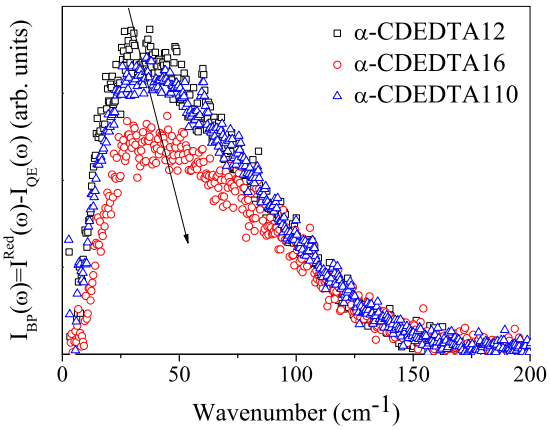


**Fig. 3.** Reduced Raman spectra of α-CDEDTA1*n* nanosponges ($n = 2, 6, 10$) after subtraction of QE contribution in the energy range 0–200 $cm^{-1}$.

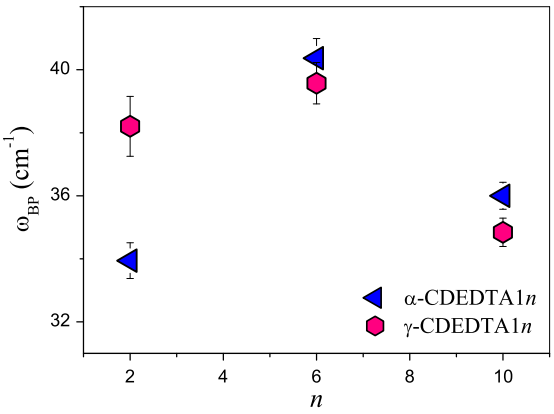


**Fig. 5.** Evolution of $\omega_{BP}$ as a function of the molar ratio *n* for different types of EDTA nanosponges: α-CDEDTA1*n* (blue left triangles) and γ-CDEDTA1*n* (pink hexagons).

The total reduced Raman intensity reported in Fig. 2 can be effectively modeled as the sum of two spectral components:

$$I^{Red}(\omega) = I_{QE}(\omega) + I_{BP}(\omega) \quad (3)$$

Where $I_{QE}(\omega)$ and $I_{BP}(\omega)$ are the respective spectral intensities.

The inspection of the experimental profiles of Fig. 2 points out significant variations of both intensity and frequency position of the BP, as a function of the *n* parameter. By the way, the intensity of the quasi-elastic signal varies, passing also from its maximum value in the spectrum of α-CDEDTA12 nanosponges to its minimum value in the α-CDEDTA16 sample.

Since in this work we are concerned only with the boson peak variations, the $I_{QE}(\omega)$ of the quasi-elastic contribution was subtracted from the total experimental profile $I^{Red}(\omega)$ by adopting a well-established fitting procedure, already successfully applied to other polymeric systems [16,17,27–29]. In the inset of Fig. 2, the best fitting results for the reduced Raman spectrum of α-CDEDTA16 are shown. The total experimental profile $I^{Red}(\omega)$ is well reproduced by the sum of a Lorentzian function, centred at zero wave number, with width $\Gamma$ and amplitude *A* to model the QE contribution (dashed line), and a log-normal distribution function that well describes the shape and the position of the BP with width *W*, amplitude *B* and peak frequency $\omega_{BP}$ (continuous line).

$$I^{Red}(\omega) = \frac{A\Gamma}{\Gamma^2+\omega^2} + B\exp\left\{-[\ln(\omega/\omega_{BP})]^2/2W^2\right\} \quad (4)$$

It is noteworthy that the choice of the log-normal function, although arbitrary, provides a suitable method to estimate in more quantitative way the position of the maximum of BP [16,17,27–31].

The data handling described above has been applied to the Raman spectra of both α- and γ- EDTA1*n* nanosponges.

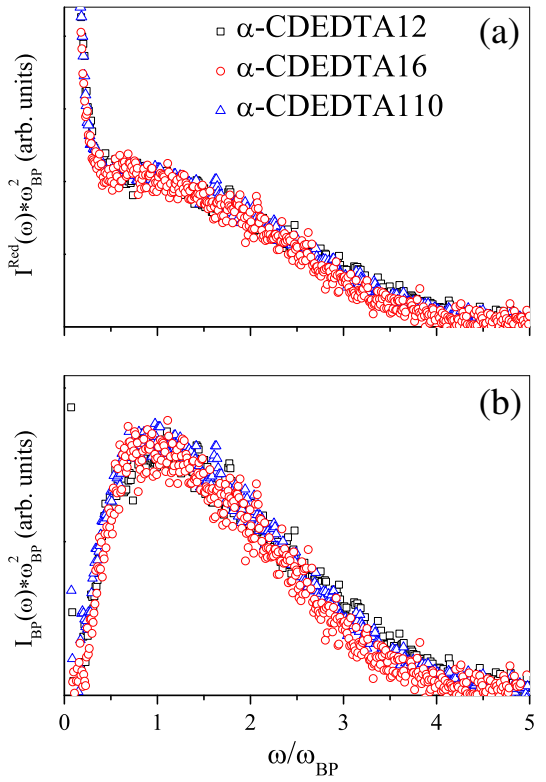


**Fig. 4.** Master curve of the Boson peak for the reduced Raman intensity before (a) and after (b) the subtraction of QE contribution, obtained as discussed in the text for α-CDEDTA1*n* nanosponges ($n = 2, 6, 10$).

## 4. Discussion

Fig. 3 displays the Stokes components of the reduced Raman spectra of the three different samples of α-CDEDTA1*n* nanosponges, in the spectral range 0–200 $cm^{-1}$, obtained after the subtraction of QE contribution, which has been carefully carried out following the same method discussed in Ref. [16,17]. The profiles obtained in this way correspond only to the intensity $I_{BP}(\omega)$ of the vibrational component of the reduced spectra.

It turns out clearly evident that the boson peak shifts toward higher wave numbers and decreases in intensity when the parameter *n* passes from 2 to 10 and then to 6. It should be pointed out that the overall evolution of the vibrational component, obtained after subtraction of the QE contribution, is the same as the one observed for the reduced Raman spectra of Fig. 2, thus confirming that the described subtraction procedure of the QE contribution does not affect the final results.

As already widely demonstrated in previous work papers [16,27–30], a clear relationship exists between the changes in the frequency and intensity of the BP and the transformation of the elastic properties of the material over a mesoscopic length scale. As a matter of fact, it has been shown that the position of the maximum of BP tends to move to higher energies when the stiffness of the amorphous system increases, as induced by pressure [27–29], density [30,32] or increasing of connectivity [16,17]. In particular, in the case of cyclodextrin-based polymers, it has been observed that the evolution of $\omega_{BP}$ as a function of the cross-linking degree of the polymeric network is in fair agreement with the trend observed for the Brillouin sound velocity measured on the same samples [16].

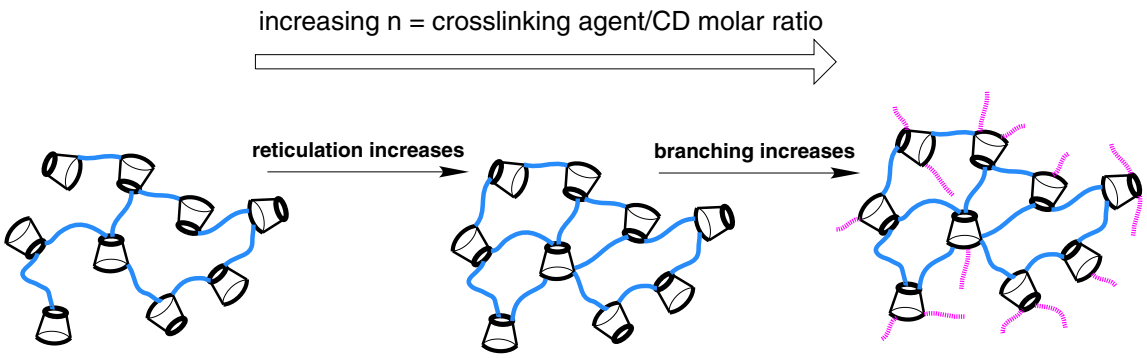


**Fig. 6.** Schematic picture representing the effect of increasing of the parameter $n$ on the structural properties of CDNS polymer network.

The behaviour of $\omega_{BP}$ observed for α-CDEDTA1$n$ nanosponges in Fig. 3 is consistent with the change in the elastic properties of these systems, which appears to show a maximum in the stiffness of the polymeric matrix corresponding to $n = 6$.

This result can be further confirmed by the analysis of the shape of the BP as a function of molar ratio $n$, which is achieved by rescaling the frequency axis of the Raman spectra in terms of $\upsilon = \omega/\omega_{BP}$. To this aim, in order to warrant the invariance of the density of vibrational states of the materials, we are forced to put $g(\omega)d\omega = g(\upsilon)d\upsilon$ [30]. Accordingly, the change of $x$ variable from $\omega$ to $\upsilon$ imposes that also the reduced Raman intensity must be rescaled trough to the relation [30]:

$$I(\upsilon(\omega)) = I^{Red}(\omega) \times {\omega_{BP}}^2 \quad (5)$$

The so-rescaled spectra reproducing the Raman spectra and the profile of the resulting vibrational components, obtained after subtraction of the QE contribution, are shown in Fig. 4(a) and (b), respectively, for α-CDEDTA1$n$ nanosponges. The values of $\omega_{BP}$ used to rescale both the frequency and the intensity of the spectra were preliminarily estimated by using the data fitting procedure based on Eq. (4).

It is worth noticing that, within the experimental error, the spectra corresponding to different samples of EDTA nanosponges are perfectly overlapped, collapsing into a single master curve, clearly evident in both the panels of Fig. 4. It should be pointed out that its master curve is obtained without any adjustable parameter.

The existence of a master curve for BP, in agreement with the results obtained on other glass-former systems [28,30,33,34], gives evidence that the spectral shape of the BP is essentially the same for the three different types of α-CDEDTA1$n$ nanosponges. This finding is consistent with the conclusion that the transformation of BP is only determined by the changes occurring in the elastic properties of the material, independently of the modifications of the microscopic structure of the sample.

Finally, Fig. 5 shows the evolution of $\omega_{BP}$ for the two different types of nanosponges obtained by polymerization of α- and γ-CD with the cross-linking agent EDTA as a function of the parameter $n$.

The plots show a similar dependence on $n$ of the stiffness of polymeric network with a maximum of the rigidity of the systems which corresponds to a six-fold excess of cross-linker EDTA with respect to the monomer α- or γ-CD. This finding is in agreement with the behaviour observed for other cyclodextrin-based polymers obtained by polymerization of β-CD with the same cross-linking agent EDTA [17] and with pyromellitic dianhydride (PMA), in dry [15,16,18] and hydrated state [35]. In fact, in all these systems, a triggering of stiffness and cross-linking degree (i.e., connectivity) was systematically observed in correspondence of the molar ratio $n = 6$. The rationale of this experimental finding could rely on two competing effects, as schematized in Fig. 6: on one side, the cross-linker molar excess boosts the reactivity, leading to reticulation and formation of three-dimensional network mediated by both covalent bonds (ester linkages) and non-covalent interactions (hydrogen bonds). Otherwise, beyond a six-fold excess of EDTA or PMA, the addition of cross-linkers does not result in a further growth of the polymeric network but rather increases the branching of cyclodextrin units and introduces some destructuring effects, mainly of entropic nature, that do not favor the establishment of hydrogen bonds.

## 5. Conclusions

The evolution of the low-frequency vibrational spectra of cyclodextrin-based cross-linked polymers was here investigated as a function of the type of CD monomeric unit (α- or γ-CD) and the relative amount of cross-linking agent with respect to CD. Significant changes in the intensity and frequency position of the boson peak were observed, mainly depending on the parameter $n$, in agreement with the results obtained on other cyclodextrin-based polymers. By using the BP maximum as a physical descriptor of the stiffness properties of the material, we find an upper limit in the rigidity of EDTA nanosponges polymeric network corresponding to a six-fold excess of cross-linker with respect to the monomer CD. This result confirms that the effect of saturation for the three-dimensional growth of the polymer is triggered for values of $n > 6$. Finally, the existence of a scaling law for the BP spectral shape was verified, supporting that the transformation of BP is only determined by the changes occurring in the elastic properties of the material.

## References

[1] F. Trotta, W. Tumiatti, R. Cavalli, O. Zerbinati, C. M. Roggero, R. Vallero, Patent number WO 06/002814 (2006).
[2] F. Trotta, W. Tumiatti, Patent number WO 03/085002 (2003).
[3] F. Trotta, M. Zanetti, R. Cavalli, Beilstein J. Org. Chem. 8 (2012) 2091.
[4] S. Li, W.C. Purdy, Chem. Rev. 92 (1992) 1457.
[5] J. Szejtli, Chem. Rev. 98 (1998) 1743.
[6] In: M.L. Bender, M. Komiyama (Eds.), Cyclodextrin Chemistry, Springer-Varlag, New York, 1978.
[7] L. Seglie, K. Martina, M. Devecchi, C. Roggero, F. Trotta, V. Scariot, Postharvest Biol. Technol. 59 (2011) 200.
[8] D. Li, M. Ma, Clean Prod. Process. 2 (2000) 112.
[9] S. Swaminathan, L. Pastero, L. Serpe, F. Trotta, P.R. Vavia, D. Aquilano, M. Trotta, G. Zara, R. Cavalli, Eur. J. Pharm. Biopharm. 74 (2010) 193.
[10] D. Lembo, S. Swaminathan, M. Donalisio, A. Civra, L. Pastero, D. Aquilano, P. Vaviac, F. Trotta, R. Cavalli, Int. J. Pharm. 443 (2013) 262.
[11] E. Memisoglu-Bilensoy, I. Vural, A. Bochot, J.M. Renoir, D. Duchene, A.A. Hincal, J. Control. Release 104 (2005) 489.
[12] R. Cavalli, A. Akhter, A. Bisazza, P. Giustetto, F. Trotta, P. Vavia, Int. J. Pharm. 402 (2010) 254.
[13] A. Vyas, S. Shailendra, S. Swarnlata, J. Incl. Phenom. Macro. Chem. 62 (2008) 23.
[14] P.K. Shende, F. Trotta, R.S. Gaud, K. Deshmukh, R. Cavalli, M. Biasizzo, J. Incl. Phenom. Macro. Chem. 74 (2012) 447.
[15] A. Mele, F. Castiglione, L. Malpezzi, F. Ganazzoli, G. Raffaini, F. Trotta, B. Rossi, A. Fontana, G. Giunchi, J. Incl. Phenom. Macro. Chem. 69 (2011) 403.
[16] B. Rossi, S. Caponi, F. Castiglione, S. Corezzi, A. Fontana, M. Giarola, G. Mariotto, A. Mele, C. Petrillo, F. Trotta, G. Viliani, J. Phys. Chem. B 116 (2012) 5323.

[17] V. Crupi, A. Fontana, M. Giarola, D. Majolino, G. Mariotto, A. Mele, L. Melone, C. Punta, B. Rossi, F. Trotta, V. Venuti, J. Raman Spectrosc. 44 (10) (2013) 1457.
[18] F. Castiglione, V. Crupi, D. Majolino, A. Mele, B. Rossi, F. Trotta, V. Venuti, J. Phys. Chem. B 116 (2012) 7952.
[19] F. Castiglione, V. Crupi, D. Majolino, A. Mele, B. Rossi, F. Trotta, V. Venuti, J. Phys. Chem. B 116 (2012) 13133.
[20] F. Castiglione, V. Crupi, D. Majolino, A. Mele, W. Panzeri, B. Rossi, F. Trotta, V. Venuti, J. Incl. Phenom. Macro. Chem. 75 (2013) 247.
[21] W. Kob, K. Binder, Glassy Materials and Disordered Solids: An Introduction, World Scientific, London, 2011.
[22] P. Benassi, A. Fontana, W. Frizzera, M. Montagna, V. Mazzacurati, G. Signorelli, Philos. Mag. B 71 (1995) 761.
[23] A.P. Sokolov, D. Quitmann, E. Duval, Phys. Rev. B 48 (1993) 7692.
[24] E. Fabiani, A. Fontana, U. Buchenau, J. Chem. Phys. 128 (2008) 244507.
[25] F. Trotta, W. Tumiatti, R. Cavalli, C.M. Roggero, B. Mognetti, G. Berta Nicolao, Patent number WO 09/003656 (2009).
[26] R. Shuker, R.W. Gammon, Phys. Rev. Lett. 25 (1970) 222.
[27] K. Niss, B. Begen, B. Frick, J. Ollivier, A. Beraud, A. Sokolov, V.N. Novikov, C. Alba-Simionesco, Phys. Rev. Lett. 99 (2007) 1.
[28] L. Hong, B. Begen, A. Kisliuk, C. Alba-Simionesco, V.N. Novikov, A.P. Sokolov, Phys. Rev. B 78 (2008) 134201.
[29] L. Hong, P.D. Gujrati, V.N. Novikov, A.P. Sokolov, J. Chem. Phys. 131 (2009) 1.
[30] M. Zanatta, G. Baldi, S. Caponi, A. Fontana, E. Gilioli, M. Krish, C. Masciovecchio, G. Monaco, L. Orsingher, F. Rossi, G. Ruocco, R. Verbeni, Phys. Rev. B 81 (2010) 212201.
[31] V. Crupi, A. Fontana, M. Giarola, G. Guella, D. Majolino, I. Mancini, G. Mariotto, A. Paciaroni, B. Rossi, V. Venuti, J. Phys. Chem. B 117 (2013) 3917.
[32] O. Pilla, L. Angelani, A. Fontana, J.R. Gonçalves, G. Ruocco, J. Phys. Condens. Matter 15 (2003) S995.
[33] A. Monaco, A.I. Chumakov, G. Monaco, W.A. Crichton, A. Meyer, L. Comez, D. Fioretto, J. Korecki, R. Rüffer, Phys. Rev. Lett. 97 (2006) 135501.
[34] L. Orsingher, A. Fontana, E. Gilioli, G. Carini Jr., G. Carini, G. Tripodo, T. Unruh, U. Buchenau, J. Chem. Phys. 132 (2010) 124508.
[35] V. Crupi, D. Majolino, A. Mele, B. Rossi, F. Trotta, V. Venuti, Soft Matter 9 (2013) 6457.